Supporting Information to:

Multiscale modelling of CO_2 Hydrogenation of TiO_2-supported Ni_8 Clusters: on the Influence of Anatase and Rutile Polymorphs

Lulu Chen, Ying-Ying Ye, Rozemarijn D.E. Krösschell, Emiel J. M. Hensen, Ivo A. W. Filot *

Laboratory of Inorganic Materials and Catalysis, Department of Chemical Engineering and Chemistry, Eindhoven University of Technology, P.O. Box 513, 5600 MB Eindhoven, the Netherlands

*Corresponding author.

Email:

i.a.w.filot@tue.nl (I.A.W. Filot)

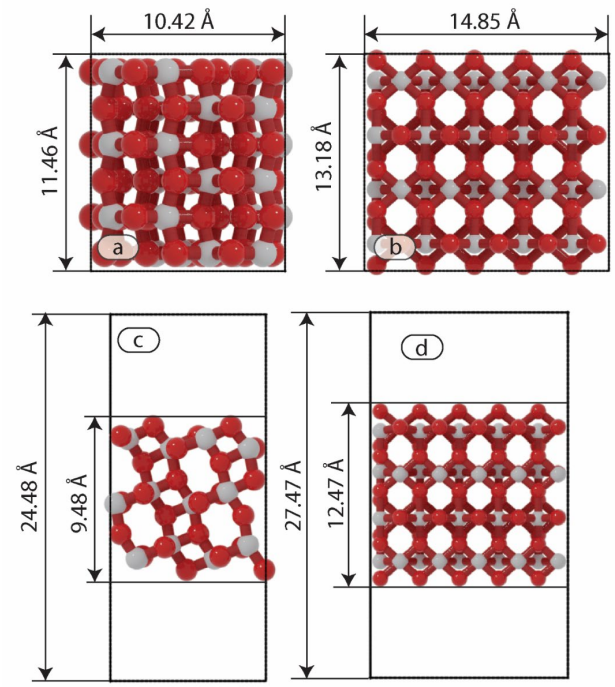

Figure S1. Surface models of TiO_2-a(101) and TiO_2-r(110). (a): the top view of TiO_2-a(101); (b): the top view of TiO_2-r(110); (c): the side view of TiO_2-a(101); (d): the side view of TiO_2-r(110). Color scheme: light gray: Ti; red: O. To enhance the visualization of the Ti atoms, the O atoms are displayed at a smaller size.

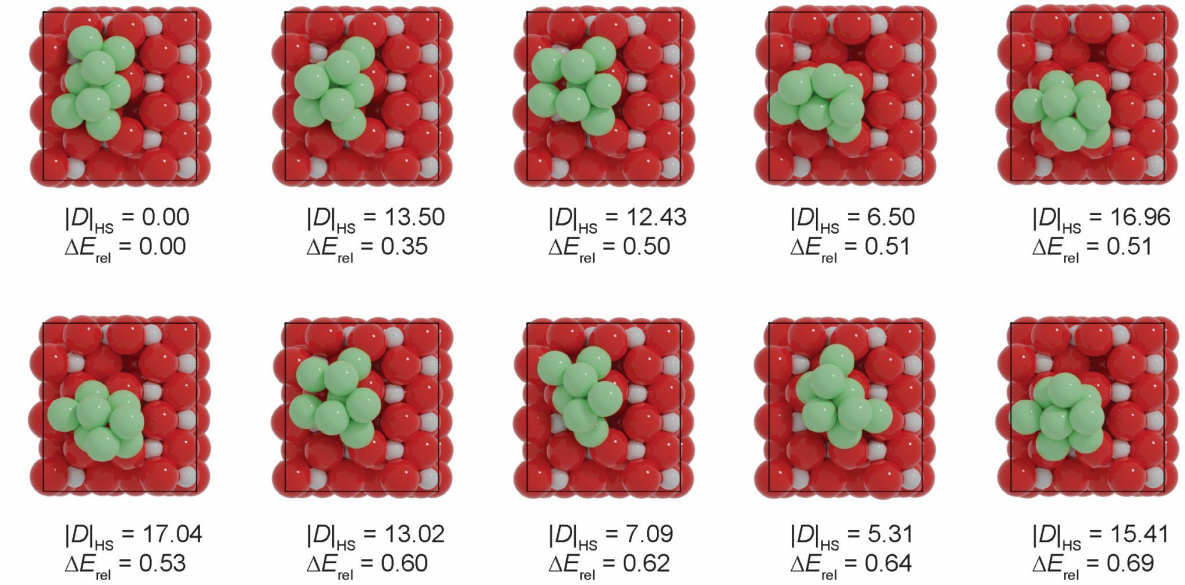

Figure S2. Ten most stable structures of Ni_8/TiO_2-a. The energy of each structure relative to the most stable structure is shown as ΔE_{rel} (measured in electron volts, eV). The similarity is indicated as the Hilbert-Schmidt norm ($|D|_{HS}$).

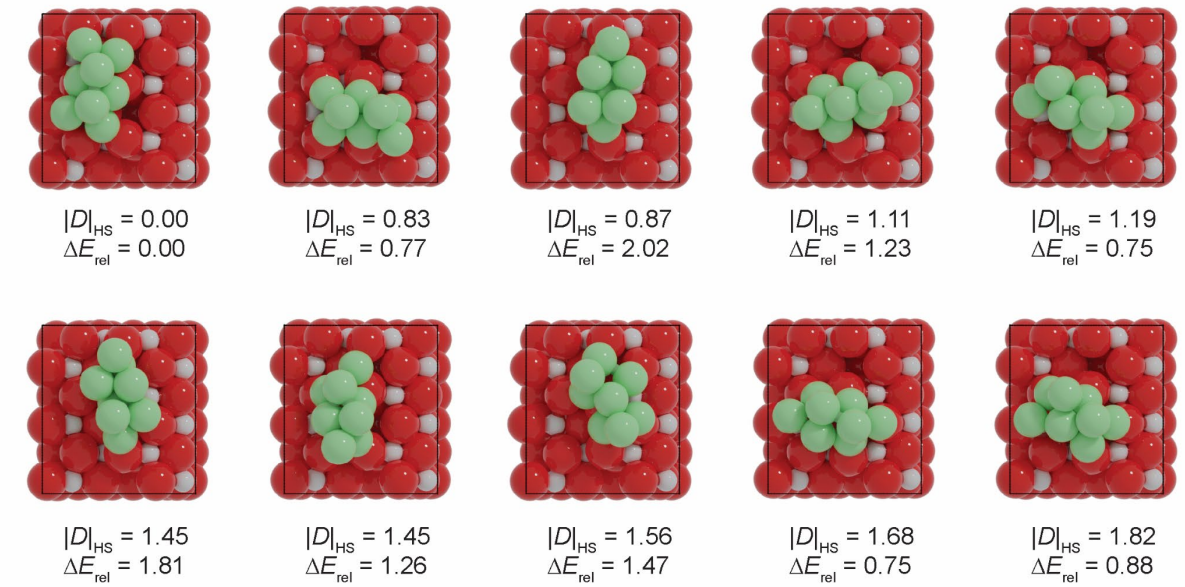

Figure S3. Comparisons of ten most similar structures of Ni_8/TiO_2-a with respect to the most stable structure. The similarity is indicated as the Hilbert-Schmidt norm ($|D|_{HS}$). The energy of each structure relative to the most stable structure is shown as ΔE_{rel} (measured in electron volts, eV).

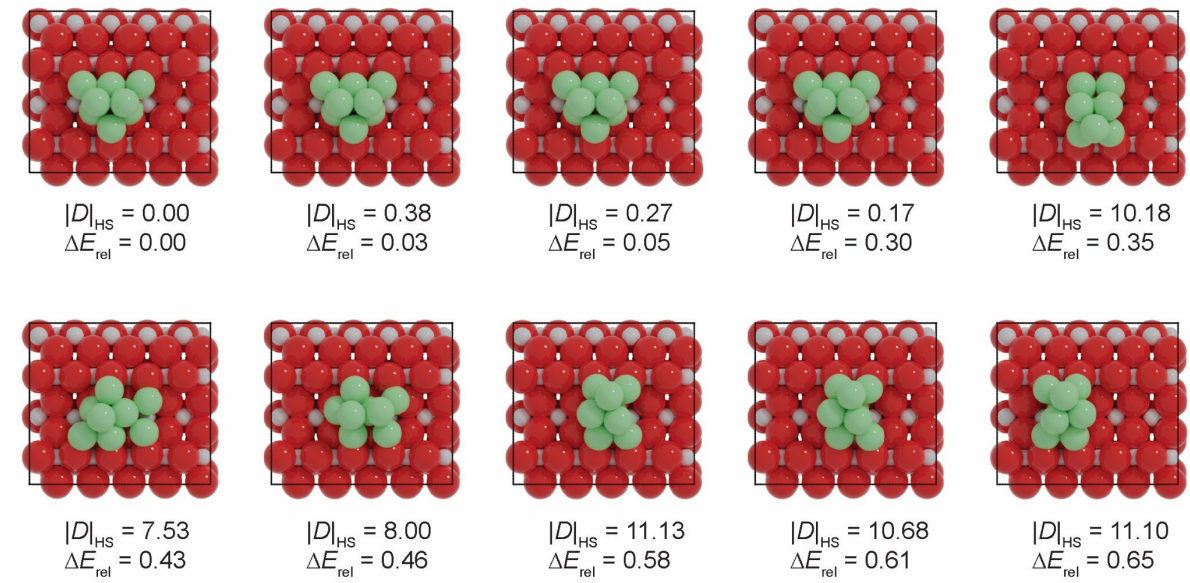

Figure S4. Ten most stable structures of Ni_8/TiO_2-r. The energy of each structure relative to the most stable structure is shown as ΔE_{rel} (measured in electron volts, eV). The similarity is indicated as the Hilbert-Schmidt norm ($|D|_{HS}$).

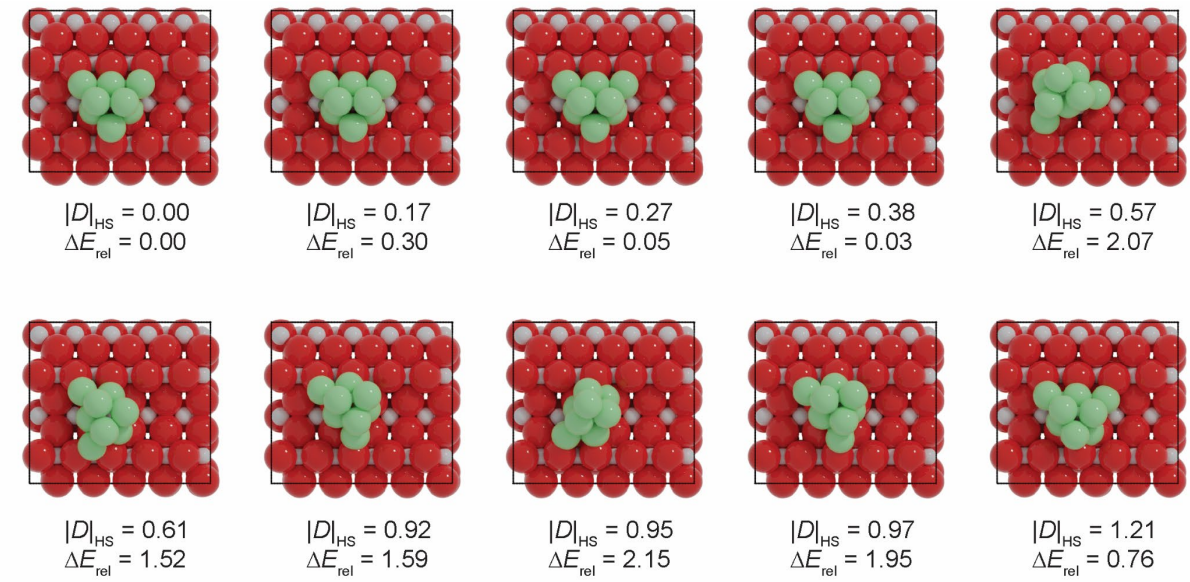

Figure S5. Comparisons of ten most similar structures of Ni_8/TiO_2-a with respect to the most stable structure. The similarity is indicated as the Hilbert-Schmidt norm ($|D|_{HS}$). The energy of each structure relative to the most stable structure is shown as ΔE_{rel} (measured in electron volts, eV).

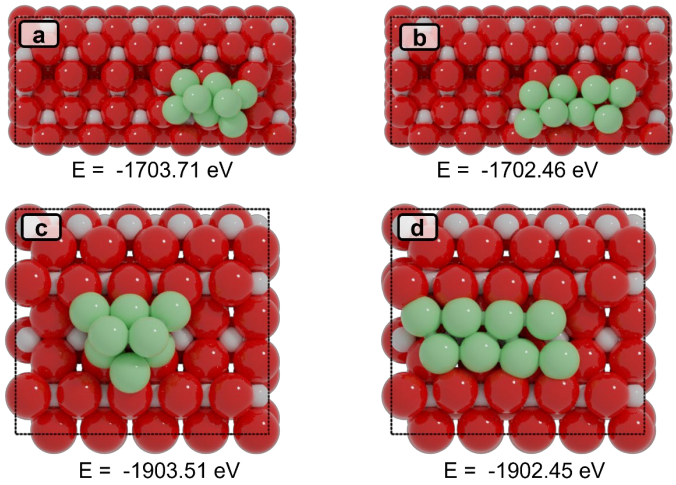

Figure S6. The configurations of 3D-Ni_8 clusters and falt Ni_8 clusters deposited on TiO_2 anatase (a and b) and rutile (c and d).

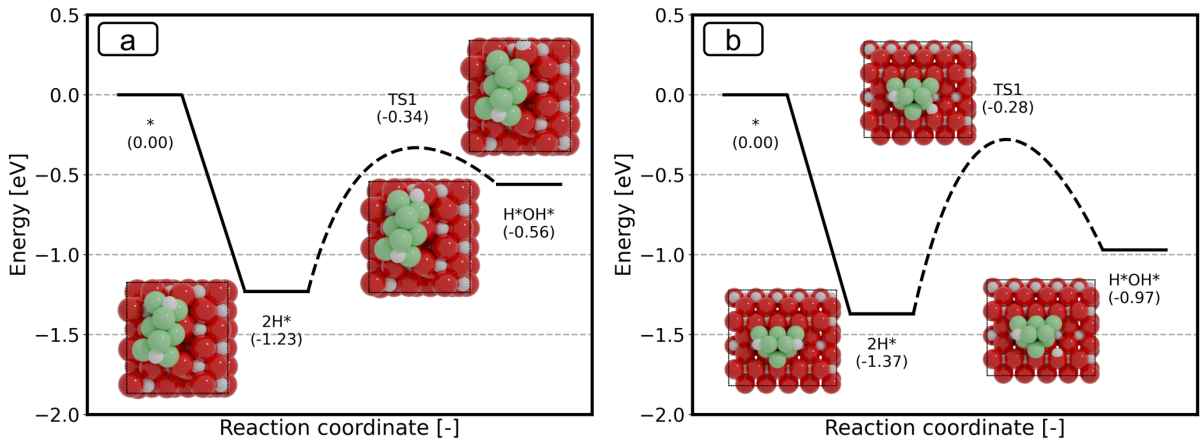

Figure S7. The energy diagrams of H spillover on Ni_8/TiO_2-a (a) and Ni_8/TiO_2-r (b).

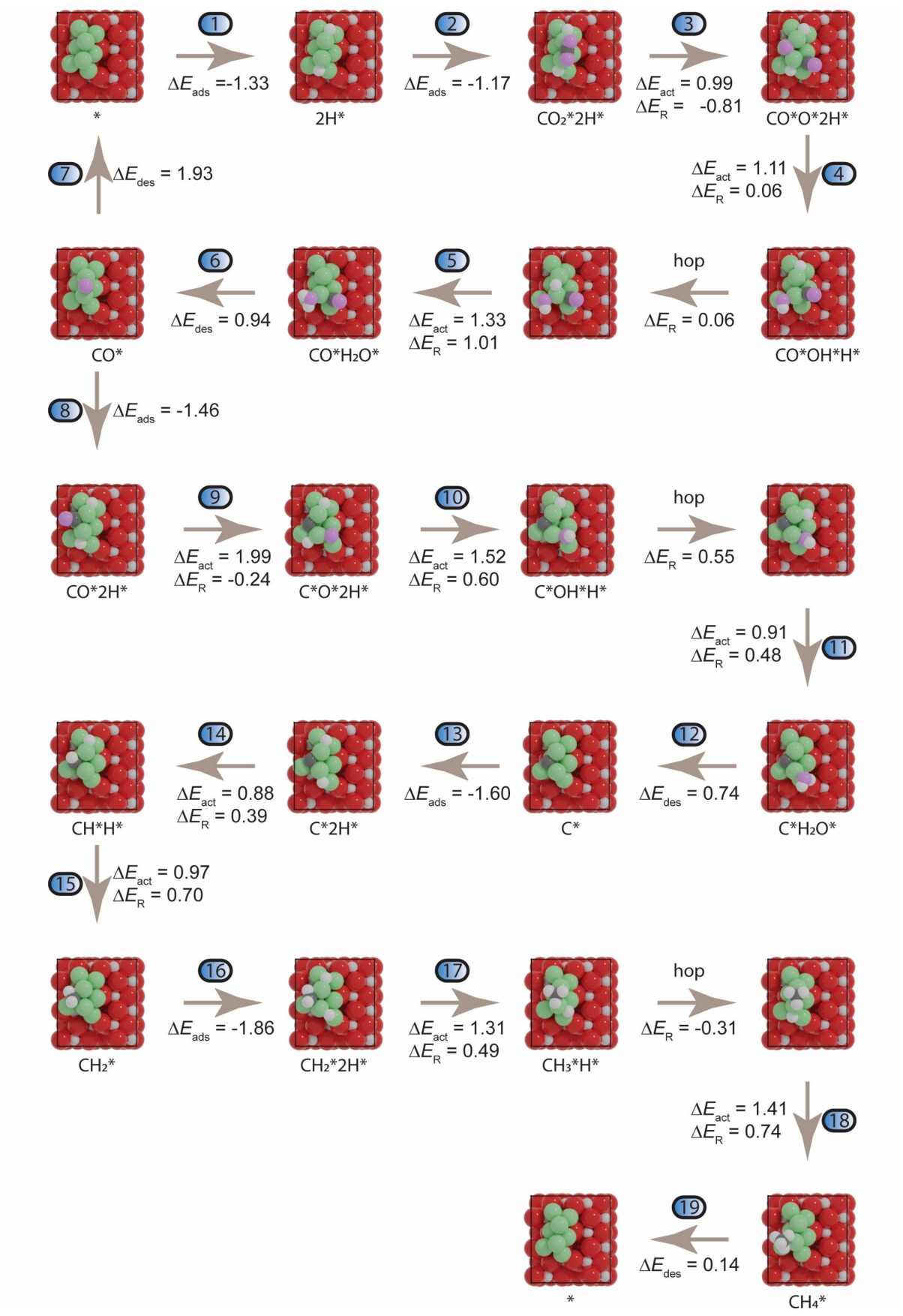

Figure S8. Configurations of CO_2 methanation on Ni_8/TiO_2-a via CH_x intermediates. Color scheme: Light gray: Ti; Red: O in support; Green: Ni; Dark gray: C; Pink: O in CO_2; White: H.

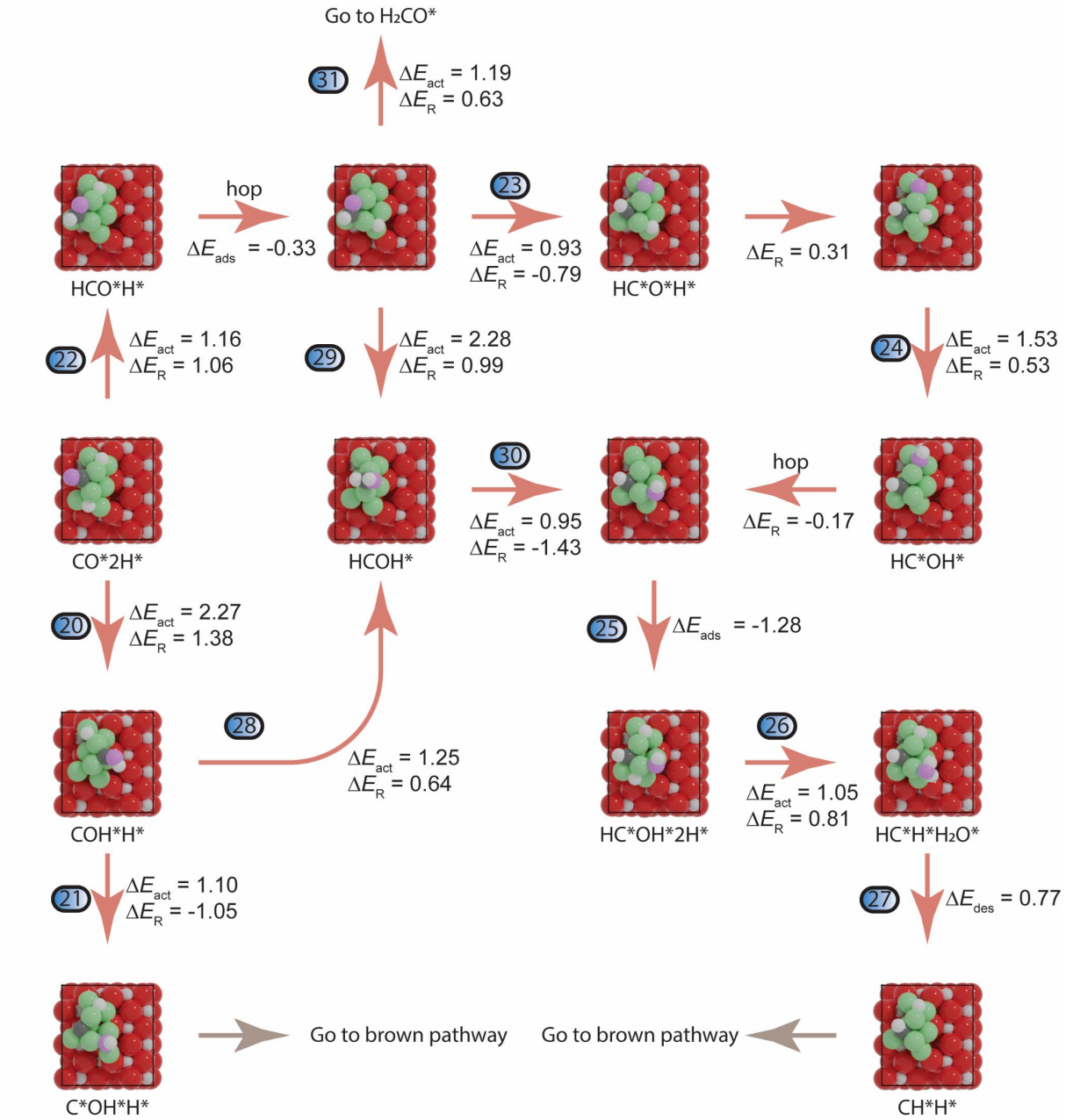

Figure S9. Configurations of CO_2 methanation on Ni_8/TiO_2-a via HCO*, COH* and HCOH* intermediates. Color scheme: Light gray: Ti; Red: O in support; Green: Ni; Dark gray: C; Pink: O in CO_2; White: H.

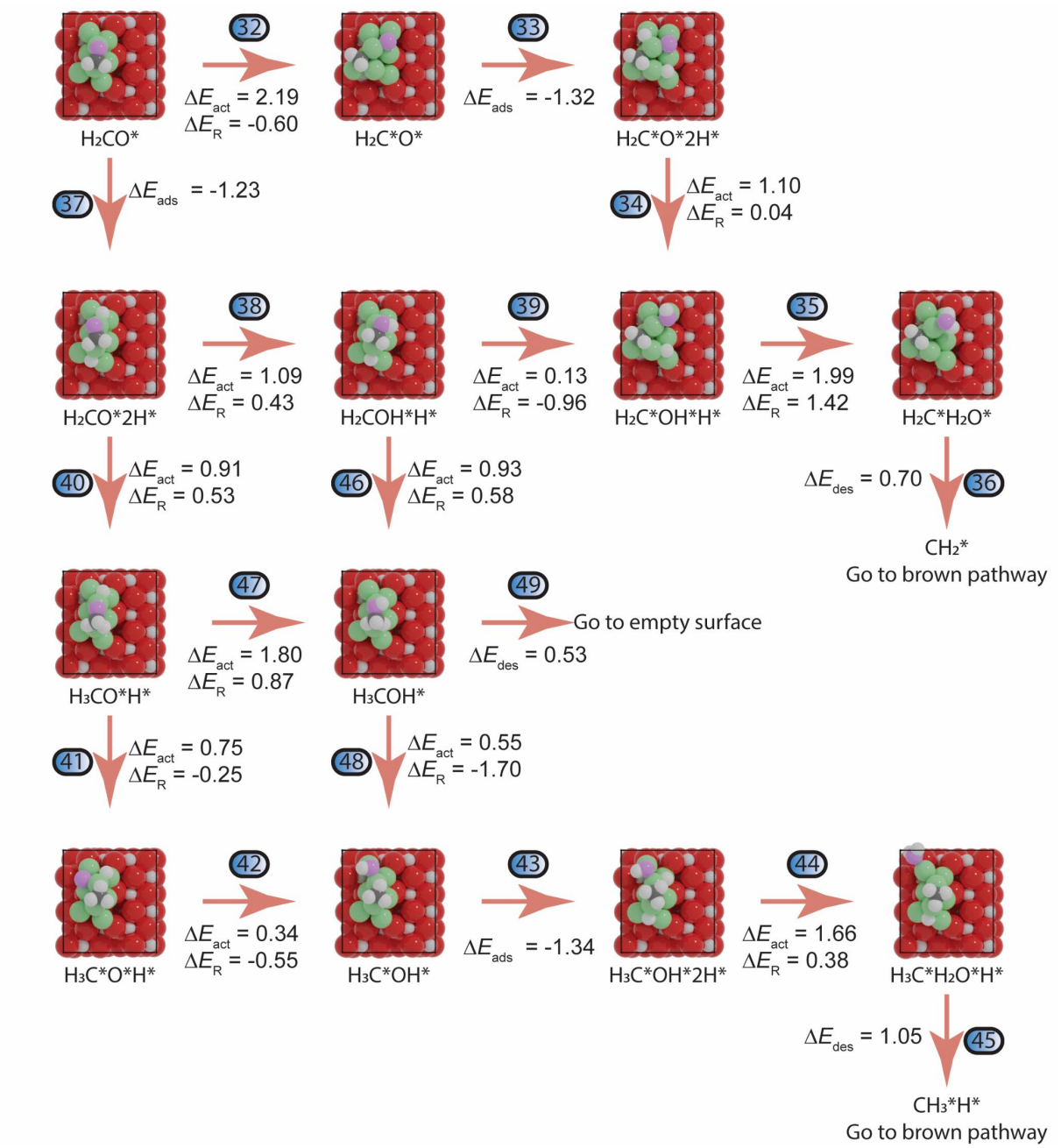

Figure S10. Configurations of CO_2 methanation on Ni_8/TiO_2-a via H_2CO^*, H_3CO^*, H_2COH^* and H_3COH^* intermediates. Color scheme: Light gray: Ti; Red: O in support; Green: Ni; Dark gray: C; Pink: O in CO_2; White: H.

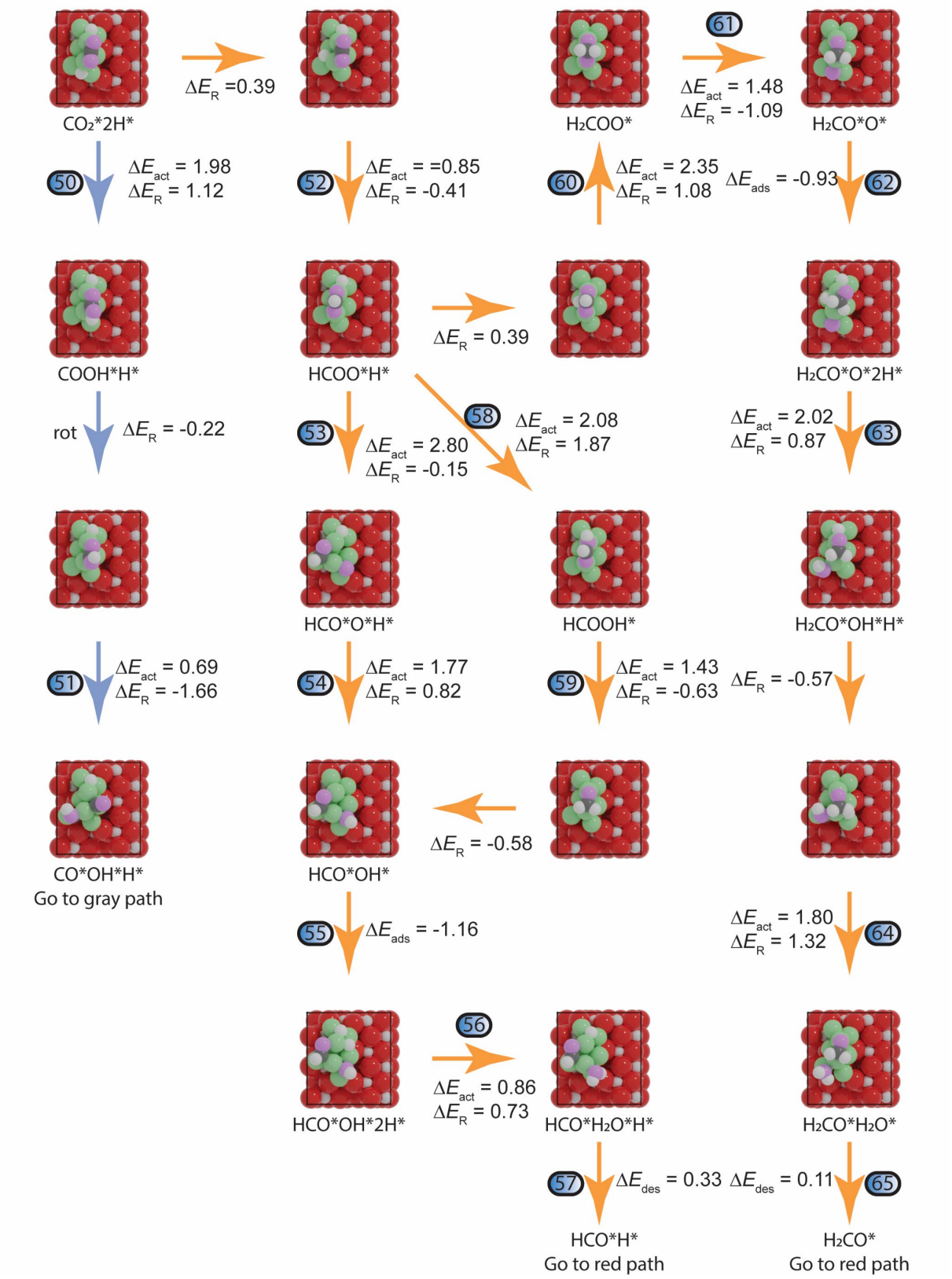

Figure S11. Configurations of H-assisted CO_2 dissociation mechanisms on Ni_8/TiO_2-a via H_xCOO^* intermediates. Color scheme: Light gray: Ti; Red: O in support; Green: Ni; Dark gray: C; Pink: O in CO_2; White: H.

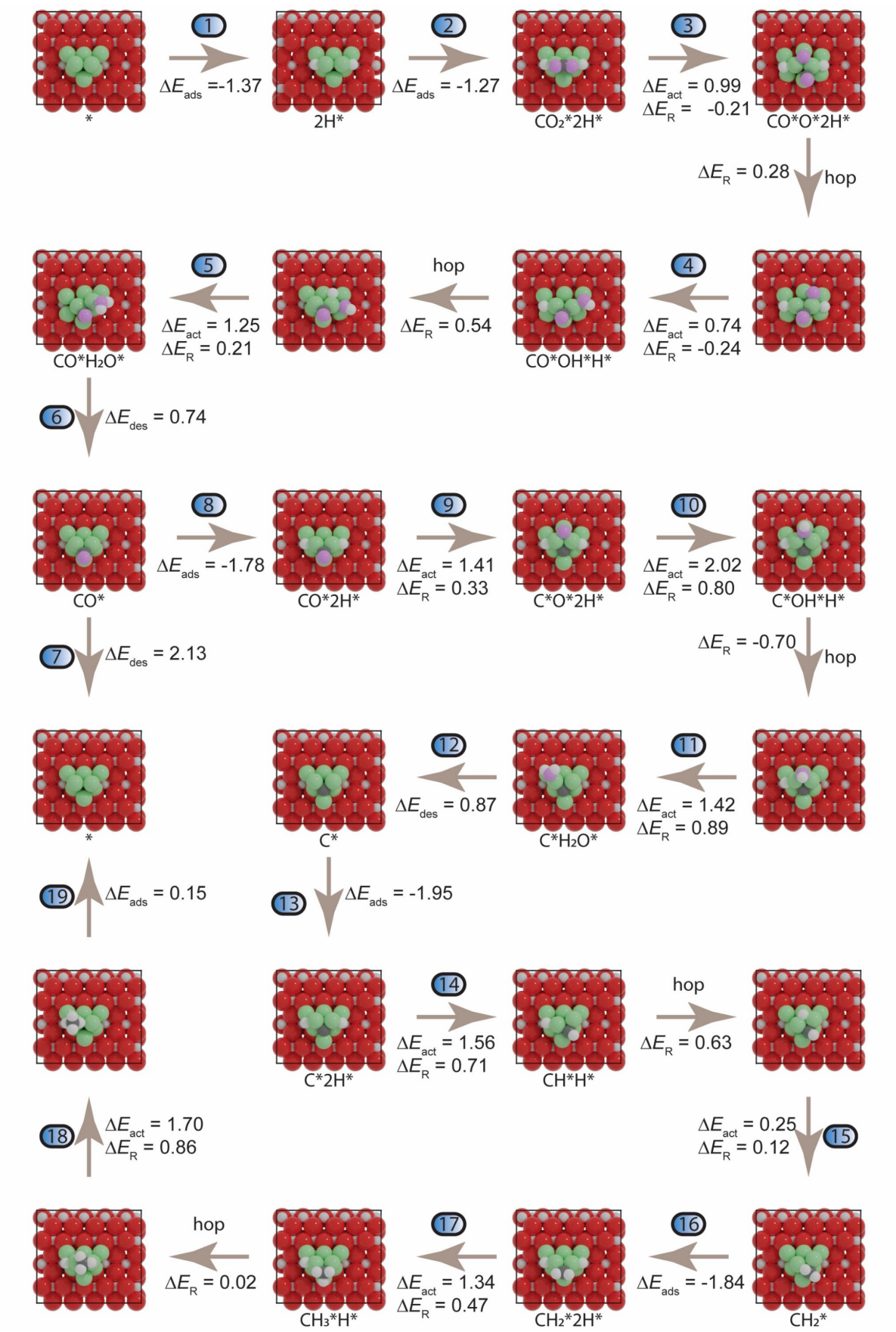

Figure S12. Configurations of CO_2 methanation on Ni_8/TiO_2-r via CH_x intermediates. Color scheme: Light gray: Ti; Red: O in support; Green: Ni; Dark gray: C; Pink: O in CO_2; White: H.

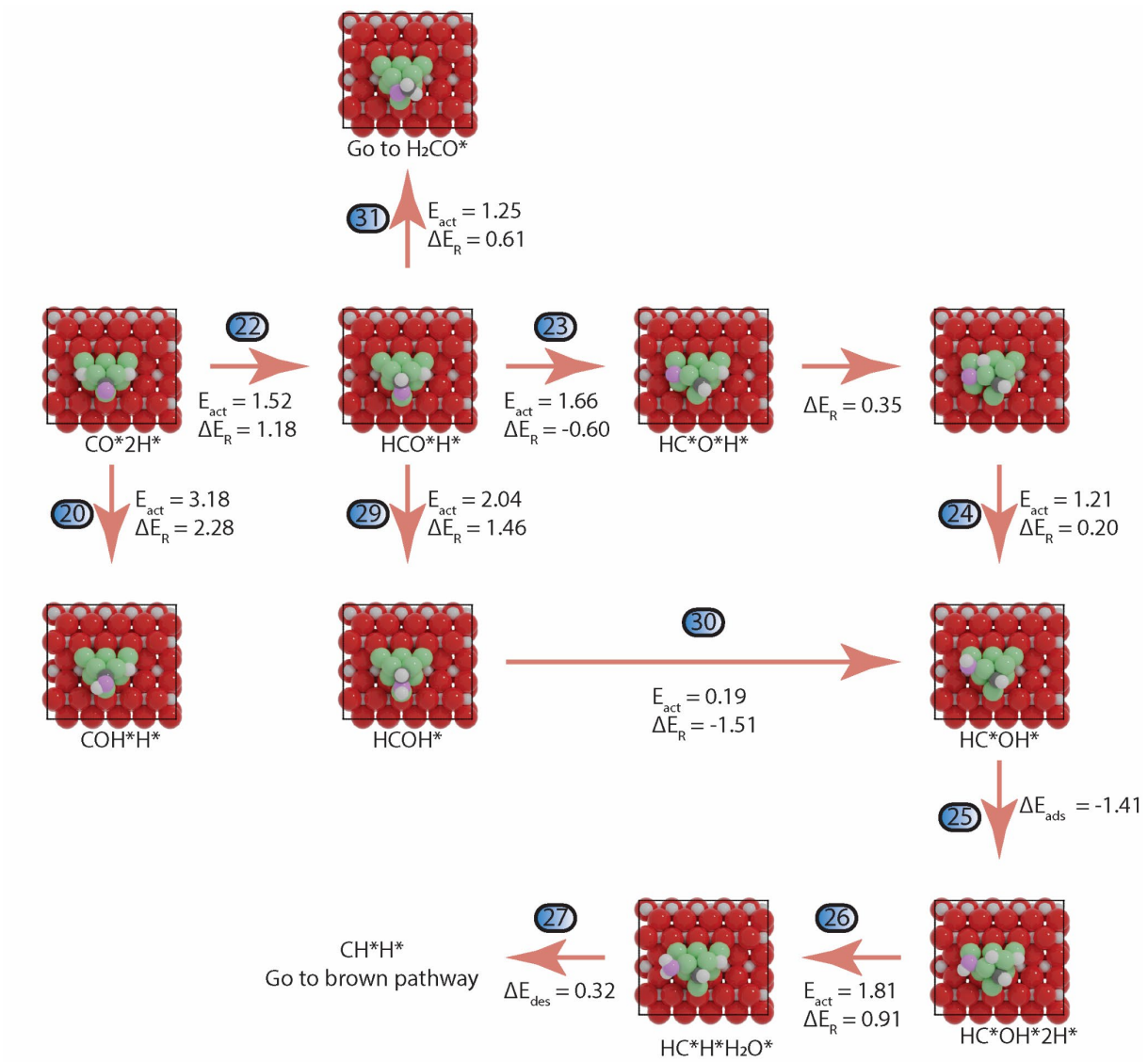

Figure S13. Configurations of H-assisted CO dissociation mechanisms on Ni_8/TiO_2-r via HCO* and HCOH* species. Color scheme: Light gray: Ti; Red: O in support; Green: Ni; Dark gray: C; Pink: O in CO_2; White: H.

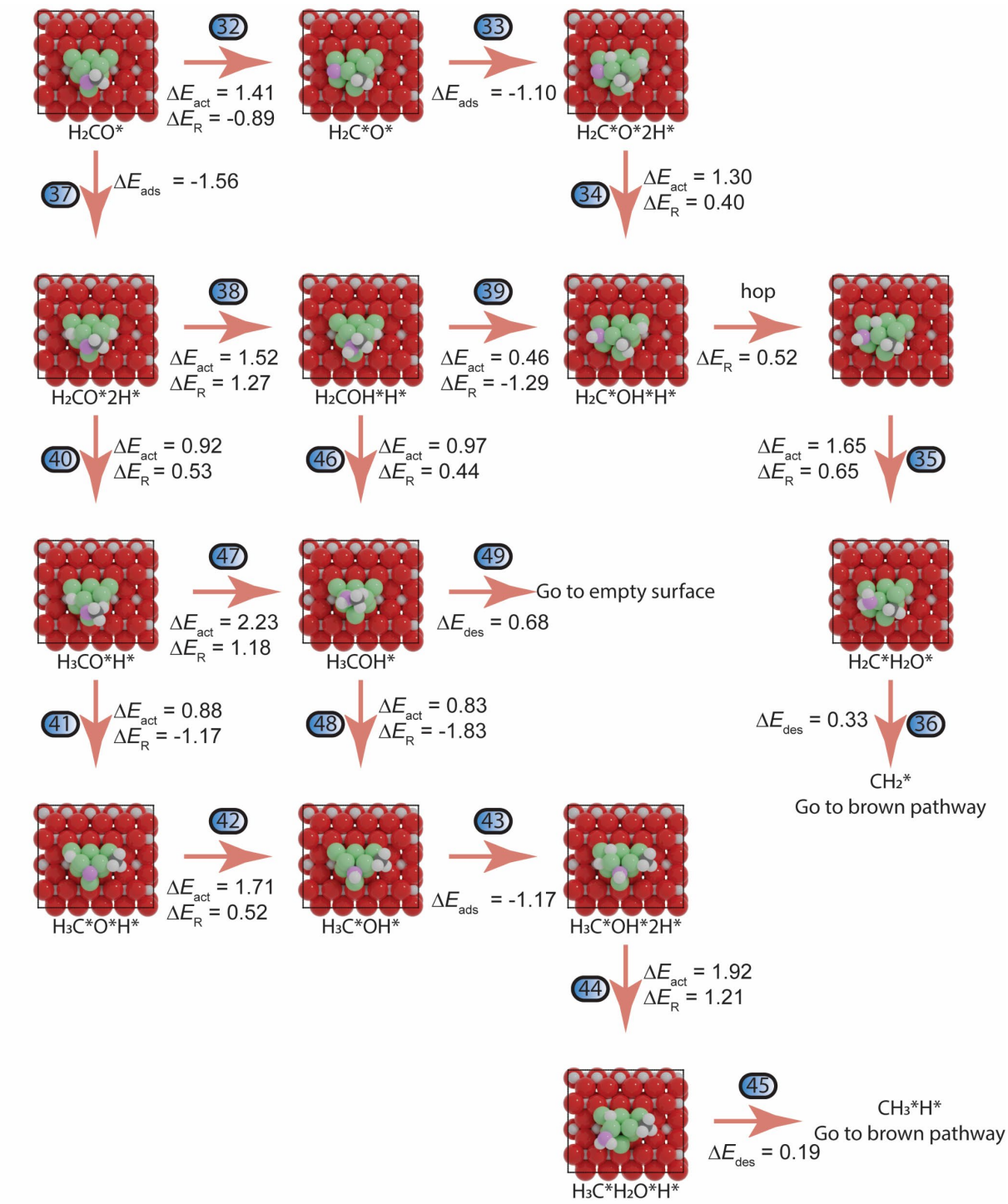

Figure S14. Configurations of H-assisted CO dissociation mechanisms on Ni_8/TiO_2-r via H_2CO*, H_2COH*, H_3CO* and H_3COH* species. Color scheme: Light gray: Ti; Red: O in support; Green: Ni; Dark gray: C; Pink: O in CO_2; White: H.

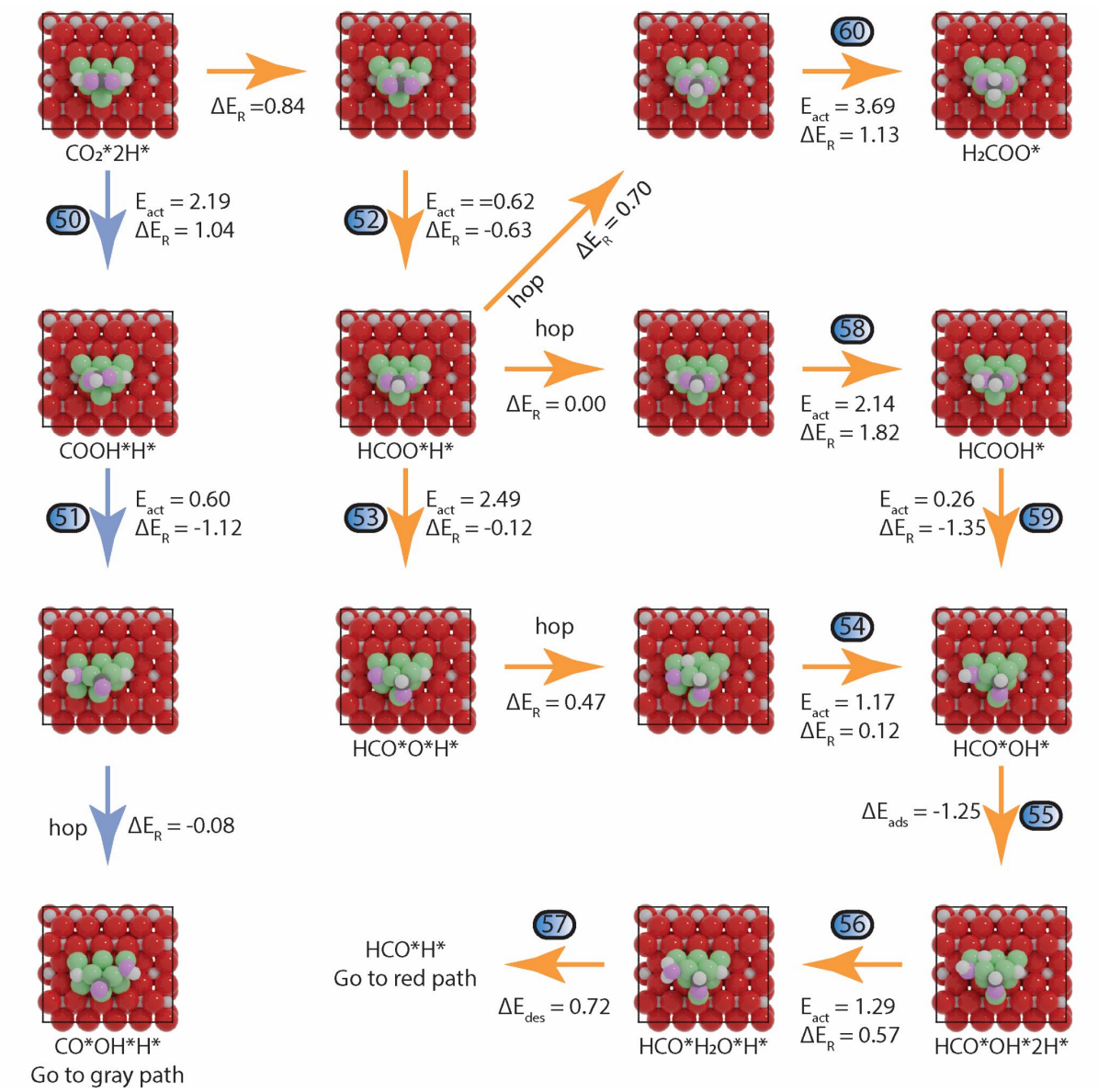

Figure S15. Configurations of H-assisted CO_2 dissociation mechanisms on Ni_8/TiO_2-r via H_xCOO^* intermediates. Color scheme: Light gray: Ti; Red: O in support; Green: Ni; Dark gray: C; Pink: O in CO_2; White: H.

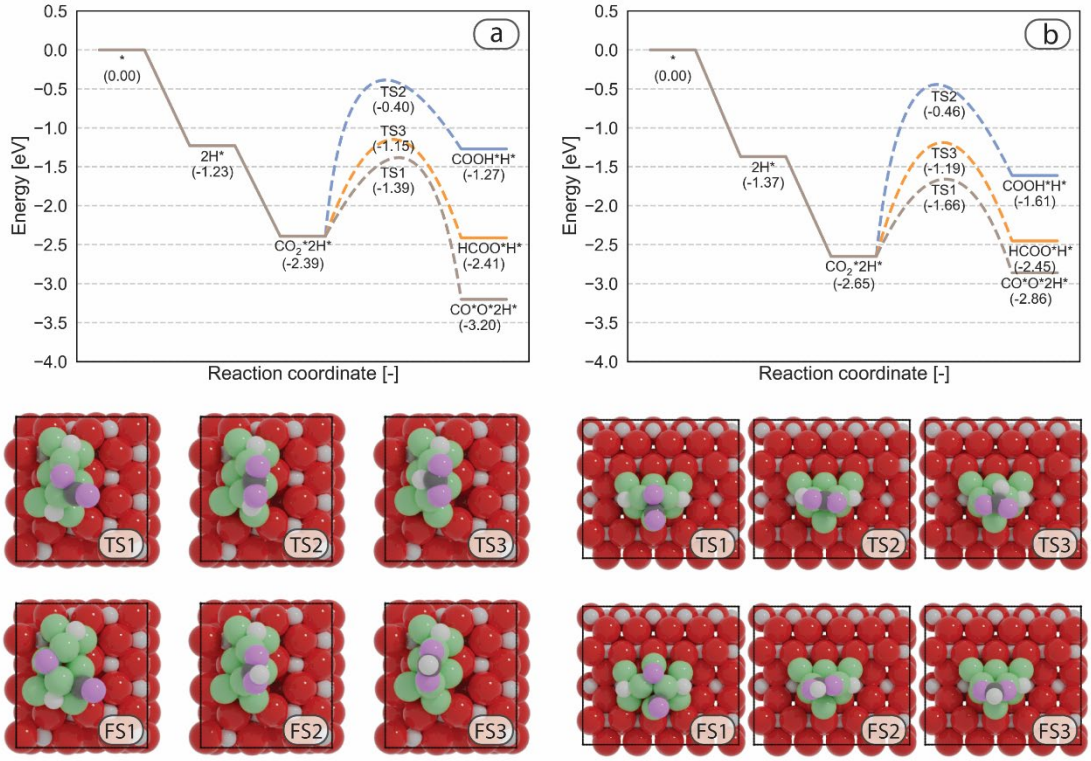

Figure S16. Reaction energy diagram of CO_2 activation on (a) Ni_8/TiO_2-a and (b) Ni_8/TiO_2-r. Direct CO_2 dissociation, COOH formation and HCOO formation are shown with brown, blue and orange lines, respectively. The corresponding configurations of transition states and final states are displayed below the energy diagram. TS1 and FS1 correspond to the transition state and final state of CO_2 direct dissociation. TS2 and FS2 represent the transition state and final state of COOH formation. TS3 and FS3 denote the transition state and final state of HCOO formation.

Section S1: Pathway Involving H_xCO_2 Intermediates for Ni_8/TiO_2-anatase

The final part of the kinetic network, corresponding to the blue and orange section in Figure 5, branches out from the direct CO_2 dissociation pathway (between R2 and R3) and pertains to the elementary reaction steps involving H_xCO_2 intermediates. The activation and reaction energy for COOH* formation from CO_2 (R50) is ΔE_{act} = 1.98 eV and ΔE_R = 1.12 eV, respectively. COOH* decomposes into CO* and OH* (R51) which is the same as CO*OH*H* in the CH_x intermediates pathway. The dissociation of COOH* needs to overcome an activation energy of 0.69 eV and this step is exothermic by 1.66 eV. The pathway from CO_2*2H* to CO*OH*H* through the direct CO_2 dissociation has an activation energy of 1.11 eV, whereas the COOH* pathway exhibits a higher activation energy of 1.98 eV.

To obtain HCOO*, H* first migrates from $H_{1\text{-}6\text{-}7}$ to $H_{1\text{-}2\text{-}7}$ site (ΔE_R = 0.39 eV) such that H gets close to the C atom in adsorbed CO_2. Next, HCOO* formation is exothermic by 0.41 eV overcoming an activation energy of 0.85 eV. Including the energy for H migration, the overall activation and reaction energies for HCOO* formation (R52) is ΔE_{act} = 1.24 eV and ΔE_R = -0.02 eV, respectively.

HCOO*H* can either dissociate in HCO*O*H* (R53, ΔE_{act} = 2.80 eV, ΔE_R = -0.15 eV), or become hydrogenated to form HCOOH* (R58, ΔE_{act} = 2.08 eV, ΔE_R = 1.87 eV) or H_2COO* (R60, ΔE_{act} = 2.74 eV, ΔE_R = 1.47 eV). The dissociated O* in HCO*O*H*reacts with H* forming an OH* (R54) with an activation energy of 1.77 eV and a reaction energy of 0.82 eV. The OH* species can also be obtained through the dissociation of HCOOH* (R59, ΔE_{act} = 1.43 eV, ΔE_R = -1.21 eV). The OH* is then hydrogenated to H_2O* in the presence of H*, which is provided by the adsorption of H_2 (R55, ΔE_{ads} = -1.16 eV). The subsequent formation of H_2O* (R56) is endothermic by 0.73 overcoming an activation energy of 0.86 eV. The desorption of H_2O (R57) generates the same configuration of HCO*H* in the H-assisted CO dissociation mechanism with a desorption energy of 0.33 eV.

The dissociation of H_2COO* results in the formation of H_2CO* and O* (R61) with an activation energy of 1.48 eV and an exothermic reaction energy of 1.09 eV. The adsorption of H_2 on this surface is exothermic by -0.93 eV (R62). The O* subsequently reacts with these two H* forming OH* (R63, ΔE_{act} = 2.02 eV, ΔE_R = 0.30 eV) and H_2O* (R64, ΔE_{act} = 1.80 eV, ΔE_R = 1.32 eV). Finally, H_2O desorbs leaving only H_2CO* on the cluster (R65, ΔE_{des} = 0.11 eV), which is the same as the H_2CO* species in the H-assisted CO dissociation pathway.

Section S2: Pathway Involving H_xCO_2 Intermediates for Ni_8/TiO_2-rutile

The last section involves H-assisted CO_2 dissociation via H_xCO_2 intermediates as depicted by the blue and orange section in Figure 6. Hydrogenation of CO_2 leads to formation of COOH* (R50, ΔE_{act} = 2.19 eV, ΔE_R = 1.04 eV) or HCOO* (R52, ΔE_{act} = 1.46 eV, ΔE_R = -0.20 eV). COOH* can dissociate to yield CO* and OH* (R51, ΔE_{act} = 0.60 eV, ΔE_R = -1.04 eV), which are located at $B_{7\text{-}8}$ and $H_{1\text{-}4\text{-}7}$ sites, respectively. This configuration closely resembles the CO*OH*H* intermediate in the CH_x-intermediates pathway, with a negligible energy difference of -0.08 eV. Dissociation of HCOO* generates HCO* and O* (R53, ΔE_{act} = 2.49 eV, ΔE_R = -0.12 eV), resulting in the presence of HCO*, O* and H* on the surface. The H* migrates from $H_{1\text{-}4\text{-}7}$ to $H_{2\text{-}7\text{-}8}$ (ΔE_R = 0.47 eV), followed by a reaction between O* and H* to generate OH* (R54, ΔE_{act} = 1.17 eV, ΔE_R = 0.12 eV). This configuration can alternatively be obtained through the formation (R58, ΔE_{act} = 2.14 eV, ΔE_R = 1.82 eV) and dissociation of HCOOH* (R59, ΔE_{act} = 0.26 eV, ΔE_R = -1.35 eV). After adsorption of H_2 (R55, ΔE_{ads} = -1.25 eV), OH* can be hydrogenated to form H_2O* (R56, ΔE_{act} = 1.29 eV, ΔE_R = 0.57 eV) which can desorb with an associated desorption energy of 0.72 eV, leaving HCO*H* on the surface and linking back to the red segment of the kinetic network. Finally, the hydrogenation of HCOO* to H_2COO* (R60) requires an activation energy of 4.39 eV including the migration of H*. We consider this barrier to be prohibitively large and therefore did not consider the subsequent H_2COO* dissociation and O* hydrogenation.

Table S1. Activation energies of CO_2 methanation on Ni_8/TiO_2-a and Ni_8/TiO_2-r. The reaction numbers are the same as in Figure 4 and Figure 7. The values are given in eV.

No.	Elementary reaction	Ni_8/TiO_2 anatase (101)		Ni_8/TiO_2 rutile (110)	
		$\Delta E_{act, forward}$	$\Delta E_{act, backward}$	$\Delta E_{act, forward}$	$\Delta E_{act, backward}$
CO_2* → CO* → C* → CH_4					
R1	H_2 + * ↔ 2H**	0	1.23	0	1.37
R2	CO_2 + 2H* ↔ CO_2*2H*	0	1.16	0	1.27
R3	CO_2*2H* ↔ CO*O*2H*	0.99	1.80	0.99	1.20
R4	CO*O*2H* ↔ CO*OH*H*	1.40	1.34	1.03	0.98
R5	CO*OH*H* ↔ CO*H_2O*	1.39	0.31	1.79	1.04
R6	H_2O + CO* ↔ CO*H_2O*	0	0.94	0	0.74
R7	CO + * ↔ CO*	0	1.93	0	2.13
R8	CO* + H_2 ↔ CO*2H*	0	1.46	0	1.78
R9	CO*2H* ↔ C*O*2H*	1.99	2.23	1.41	1.08
R10	C*O*2H* ↔ C*OH*H*	1.52	0.92	2.02	1.92
R11	C*OH*H* ↔ C*H_2O*	1.46	0.43	1.42	0.53
R12	H_2O + C* ↔ C*H_2O*	0	0.74	0	0.87
R13	H_2 + C* ↔ C*2H*	0	1.60	0	1.95
R14	C*H_2* ↔ CH*H*	0.88	0.49	1.56	0.85
R15	CH*H* ↔ CH_2*	0.97	0.27	0.85	0.13
R16	H_2* + CH_2* ↔ CH_2*2H*	0	1.86	0	1.84
R17	CH_2*2H* ↔ CH_3*H*	1.31	1.13	1.34	0.88
R18	CH_3*H* ↔ CH_4*	1.41	0.67	1.72	0.84
R19	CH_4(G) + * ↔ CH_4*	0	0.14	0	0.15
CO* → COH* → H*OH*C					
R20	CO*2H* ↔ COH*H*	2.27	0.89	3.18	1.00
R21	COH*H* ↔ C*OH*H*	1.10	2.15	-	-
CO* → HCO* → CH*					
R22	CO*2H* ↔ HCO*H*	1.16	0.43	1.52	0.35
R23	HCO*H* ↔ HC*O*H*	0.9	1.71	1.66	2.26
R24	HC*O*H* ↔ HC*OH*	1.84	1.17	1.56	1.01
R25	H_2 + HC*OH* ↔ HC*OH*2H*	0	1.28	0	1.41
R26	HC*OH*2H* ↔ HC*H*H_2O*	1.05	0.24	1.81	0.90
R27	H_2O + CH*H* ↔ HC*H*H_2O*	0	0.77	0	0.32
HCOH* → HC*OH*					
R28	COH*H* ↔ HCOH*	1.25	0.61	-	-
R29	HCO*H* ↔ HCOH*	2.28	1.30	2.04	0.58
R30	HCOH* ↔ HC*OH*	0.95	2.38	0.19	1.70
HCO* → H_2CO* →H_2C*					
R31	HCO*H* ↔ H_2CO*	1.19	0.95	1.25	0.64
R32	H_2CO* ↔ H_2C*O*	2.19	2.78	2.30	1.41
R33	H_2 + H_2C*O* ↔ H_2C*O*2H*	0	1.32	0	1.10
R34	H_2C*O*2H* ↔ H_2C*OH*H*	1.10	1.06	1.30	0.89
R35	H_2C*OH*H* ↔ H_2C*H_2O*	1.99	0.57	2.17	1.00
R36	H_2O + CH_2* ↔ H_2C*H_2O*	0	0.70	0	0.33
H_2COH* → H_2C*					
R37	H_2 + H_2CO* ↔ H_2CO*2H*	0	1.23	0	1.56
R38	H_2CO*2H* ↔ H_2COH*H	1.58	0.76	1.52	0.26
R39	H_2COH*H ↔ H_2C*OH*H*	0.52	1.98	0.46	1.75
H_2CO* → H_3CO* → H_3C*					
R40	H_2CO*2H* ↔ H_3CO*H*	0.91	0.38	0.92	0.39
R41	H_3CO*H* ↔ H_3C*O*H*	0.75	1.00	0.88	2.06
R42	H_3C*O*H* ↔ H_3C*OH*	0.34	0.89	1.71	1.19
A43	H_2 + H_3C*OH* ↔ H_3C*OH*2H*	0	1.34	0	1.17
R44	H_3C*OH*2H* ↔ H_3C*H_2O*H*	1.66	1.28	1.21	1.92
R45	H_2O + CH_3*H* ↔ H_3C*H_2O*H*	0	1.05	0	0.19
H_3COH* → H_3C*					
R46	H_2COH*H ↔ H_3COH*	0.93	0.35	0.97	0.53
R47	H_3CO*H* ↔ H_3COH*	1.80	0.93	2.23	1.06
R48	H_3COH* ↔ H_3C*OH*	0.55	2.25	0.83	2.66
R49	H_3COH(G) + * ↔ H_3COH*	0	0.53	0	0.68

CO_2*2H* → COOH* → CO*OH*H					
R50	CO_2*2H* ↔ COOH*H*	1.98	1.10	2.19	1.15
R51	COOH*H* ↔ CO*OH*H*	0.69	2.35	0.60	1.72
CO_2*2H* → HCOO* → HCO*					
R52	CO_2*2H* ↔ HCOO*H*	1.24	1.26	1.46	1.26
R53	HCOO*H* ↔ HCO*O*H*	2.80	2.95	2.49	2.61
R54	HCO*O*H* ↔ HCO*OH*	1.77	0.95	1.64	1.06
R55	H_2 + HCO*OH* ↔ HCO*OH*2H*	0	1.16	0	1.25
R56	HCO*OH*2H* ↔ HCO*H_2O*H*	0.86	0.13	1.29	0.72
R57	H_2O + HCO*H*↔ HCO*H_2O*H*	0	0.33	0	0.72
HCOOH* → HCO*OH*					
R58	HCOO*H* ↔ HCOOH*	2.08	0.21	2.14	0.32
R59	HCOOH* ↔ HCO*OH*	1.43	2.64	0.26	1.61
HCOO* → H_2COO* → H_2CO*					
R60	HCOO*H* ↔ H_2COO*	2.74	1.27	-	-
R61	H_2COO* ↔ H_2CO*O*	1.48	2.57	-	-
R62	H_2 + H_2CO*O* ↔ H_2CO*O*2H*	0	0.93	-	-
R63	H_2CO*O*2H* ↔ H_2CO*OH*H*	2.02	1.72	-	-
R64	H_2CO*OH*H* ↔ H_2CO*H_2O*	1.80	0.48	-	-
R65	H_2O* + H_2CO* ↔ H_2CO*H_2O*	0	0.11	-	-
Additional CO desorption					
R66	CO + 2H* ↔ CO*2H*	0	2.17	0	2.54

Table S2. Pre-exponential factors of CO_2 methanation on Ni_8/TiO_2-a and Ni_8/TiO_2-r. Pre-exponential factors are estimated by the translation state theory at 600 K. For adsorption steps, the pressure was set to 1 bar and the area was estimated to be 2.5 Å^2. The reaction numbers are the same as in Figure 4 and Figure 7.

No.	Elementary reaction	Ni_8/TiO_2-a		Ni_8/TiO_2-r	
		$A_{forward}$	$A_{backward}$	$A_{forward}$	$A_{backward}$
CO_2* → CO* → C* → CH_4					
R1	H_2 + * ↔ 2H**	1.92×10^{08}	1.30×10^{14}	1.92×10^{08}	1.30×10^{14}
R2	CO_2 + 2H* ↔ CO_2*2H*	4.11×10^{07}	1.38×10^{16}	4.11×10^{07}	1.38×10^{16}
R3	CO_2*2H* ↔ CO*O*2H*	3.25×10^{11}	6.09×10^{11}	5.18×10^{13}	2.35×10^{14}
R4	CO*O*2H* ↔ CO*OH*H*	1.38×10^{12}	2.89×10^{12}	2.03×10^{13}	3.30×10^{11}
R5	CO*OH*H* ↔ CO*H_2O*	1.51×10^{12}	3.78×10^{11}	6.21×10^{11}	2.35×10^{10}
R6	H_2O + CO* ↔ CO*H_2O*	6.42×10^{07}	4.06×10^{14}	6.42×10^{07}	4.06×10^{14}
R7	CO + * ↔ CO*	2.06×10^{07}	3.34×10^{17}	5.15×10^{07}	2.22×10^{17}
R8	CO* + H_2 ↔ CO*2H*	1.92×10^{08}	2.51×10^{14}	1.92×10^{08}	3.78×10^{14}
R9	CO*2H* ↔ C*O*2H*	2.87×10^{12}	5.59×10^{12}	2.48×10^{11}	1.01×10^{13}
R10	C*O*2H* ↔ C*OH*H*	1.47×10^{13}	1.03×10^{13}	7.59×10^{13}	2.53×10^{13}
R11	C*OH*H* ↔ C*H_2O*	9.00×10^{12}	2.95×10^{12}	5.36×10^{12}	3.34×10^{12}
R12	H_2O + C* ↔ C*H_2O*	6.42×10^{07}	3.96×10^{15}	6.42×10^{07}	4.81×10^{14}
R13	H_2 + C* ↔ C*2H*	1.92×10^{08}	1.67×10^{14}	1.92×10^{08}	1.99×10^{14}
R14	C*H_2* ↔ CH*H*	7.08×10^{12}	5.94×10^{12}	1.50×10^{13}	1.78×10^{13}
R15	CH*H* ↔ CH_2*	9.96×10^{12}	5.90×10^{12}	1.06×10^{13}	4.70×10^{12}
R16	H_2* + CH_2* ↔ CH_2*2H*	1.92×10^{08}	1.52×10^{14}	1.92×10^{08}	2.02×10^{14}
R17	CH_2*2H* ↔ CH_3*H*	6.66×10^{12}	2.48×10^{13}	5.27×10^{12}	4.98×10^{11}
R18	CH_3*H* ↔ CH_4*	1.12×10^{13}	8.76×10^{11}	8.36×10^{11}	6.34×10^{12}
R19	CH_4(G) + * ↔ CH_4*	6.80×10^{07}	7.29×10^{14}	6.80×10^{07}	2.43×10^{15}
CO* → COH* → H*OH*C					
R20	CO*2H* ↔ COH*H*	1.32×10^{14}	6.91×10^{13}	2.62×10^{13}	4.25×10^{12}
R21	COH*H* ↔ C*OH*H*	1.48×10^{13}	3.85×10^{13}	-	-
CO* → HCO* → CH*					
R22	CO*2H* ↔ HCO*H*	9.26×10^{13}	6.18×10^{13}	6.40×10^{12}	2.29×10^{13}
R23	HCO*H* ↔ HC*O*H*	6.52×10^{12}	1.24×10^{13}	1.06×10^{13}	1.39×10^{13}
R24	HC*O*H* ↔ HC*OH*	1.05×10^{13}	1.34×10^{13}	1.78×10^{13}	1.80×10^{12}
R25	H_2 + HC*OH* ↔ HC*OH*2H*	1.92×10^{08}	1.53×10^{14}	1.92×10^{08}	1.27×10^{14}
R26	HC*OH*2H* ↔ HC*H*H_2O*	1.92×10^{13}	1.91×10^{13}	1.23×10^{14}	6.99×10^{12}
R27	H_2O + CH*H* ↔ HC*H*H_2O*	6.42×10^{07}	2.08×10^{15}	6.42×10^{07}	2.20×10^{15}
HCOH* → HC*OH*					
R28	COH*H* ↔ HCOH*	6.84×10^{12}	3.02×10^{13}	-	-
R29	HCO*H* ↔ HCOH*	1.02×10^{13}	3.55×10^{13}	1.45×10^{13}	4.76×10^{12}
R30	HCOH* ↔ HC*OH*	8.90×10^{12}	6.24×10^{12}	2.44×10^{12}	9.85×10^{11}
HCO* → H_2CO* →H_2C*					
R31	HCO*H* ↔ H_2CO*	4.21×10^{12}	1.09×10^{13}	1.35×10^{13}	2.11×10^{13}
R32	H_2CO* ↔ H_2C*O*	3.97×10^{12}	6.85×10^{11}	9.24×10^{13}	4.27×10^{13}
R33	H_2 + H_2C*O* ↔ H_2C*O*2H*	1.92×10^{08}	1.57×10^{14}	1.92×10^{08}	1.68×10^{14}
R34	H_2C*O*2H* ↔ H_2C*OH*H*	1.35×10^{13}	3.09×10^{13}	1.81×10^{13}	9.94×10^{12}
R35	H_2C*OH*H* ↔ H_2C*H_2O*	4.31×10^{13}	2.37×10^{12}	9.94×10^{12}	9.80×10^{11}
R36	H_2O + CH_2* ↔ H_2C*H_2O*	6.42×10^{07}	3.78×10^{15}	6.42×10^{07}	2.21×10^{15}
H_2COH* → H_2C*					
R37	H_2 + H_2CO* ↔ H_2CO*2H*	1.92×10^{08}	2.20×10^{14}	1.92×10^{08}	2.28×10^{14}
R38	H_2CO*2H* ↔ H_2COH*H	5.10×10^{13}	1.04×10^{14}	6.00×10^{12}	3.36×10^{12}
R39	H_2COH*H ↔ H_2C*OH*H*	1.38×10^{15}	1.26×10^{15}	6.89×10^{12}	5.53×10^{12}
H_2CO* → H_3CO* → H_3C*					
R40	H_2CO*2H* ↔ H_3CO*H*	1.08×10^{13}	2.20×10^{13}	2.55×10^{13}	6.18×10^{13}
R41	H_3CO*H* ↔ H_3C*O*H*	8.28×10^{13}	9.19×10^{11}	4.40×10^{13}	1.09×10^{13}
R42	H_3C*O*H* ↔ H_3C*OH*	1.02×10^{13}	3.69×10^{13}	2.13×10^{13}	1.81×10^{13}
A43	H_2 + H_3C*OH* ↔ H_3C*OH*2H*	1.92×10^{08}	1.69×10^{14}	1.92×10^{08}	1.98×10^{14}
R44	H_3C*OH*2H* ↔ H_3C*H_2O*H*	6.06×10^{14}	8.93×10^{12}	8.62×10^{12}	2.98×10^{12}
R45	H_2O + CH_3*H* ↔ H_3C*H_2O*H*	6.42×10^{07}	1.26×10^{16}	6.42×10^{07}	1.11×10^{15}
H_3COH* → H_3C*					
R46	H_2COH*H ↔ H_3COH*	2.25×10^{13}	5.71×10^{12}	5.92×10^{12}	2.43×10^{12}
R47	H_3CO*H* ↔ H_3COH*	3.43×10^{12}	8.74×10^{11}	2.50×10^{12}	2.38×10^{11}
R48	H_3COH* ↔ H_3C*OH*	8.52×10^{12}	1.34×10^{12}	8.33×10^{12}	1.86×10^{13}
R49	H_3COH(G) + * ↔ H_3COH*	4.81×10^{07}	2.19×10^{17}	4.81×10^{07}	1.49×10^{17}

CO_2*2H* → COOH* → CO*OH*H					
R50	CO_2*2H* ↔ COOH*H*	3.58×10^{11}	1.32×10^{13}	2.30×10^{12}	3.19×10^{12}
R51	COOH*H* ↔ CO*OH*H*	4.31×10^{13}	9.24×10^{12}	2.14×10^{13}	8.26×10^{12}
CO_2*2H* → HCOO* → HCO*					
R52	CO_2*2H* ↔ HCOO*H*	1.29×10^{12}	4.87×10^{12}	1.87×10^{13}	4.27×10^{12}
R53	HCOO*H* ↔ HCO*O*H*	3.16×10^{12}	3.18×10^{12}	4.90×10^{11}	7.42×10^{11}
R54	HCO*O*H* ↔ HCO*OH*	1.44×10^{13}	3.89×10^{12}	1.06×10^{13}	2.18×10^{12}
R55	H_2 + HCO*OH* ↔ HCO*OH*2H*	1.92×10^{08}	2.15×10^{14}	1.92×10^{08}	3.02×10^{14}
R56	HCO*OH*2H* ↔ HCO*H_2O*H*	2.84×10^{12}	1.15×10^{13}	4.90×10^{12}	3.97×10^{12}
R57	H_2O + HCO*H*↔ HCO*H_2O*H*	6.42×10^{07}	3.68×10^{15}	6.42×10^{07}	2.47×10^{15}
HCOOH* → HCO*OH*					
R58	HCOO*H* ↔ HCOOH*	2.12×10^{12}	6.80×10^{12}	6.05×10^{11}	5.36×10^{10}
R59	HCOOH* ↔ HCO*OH*	2.34×10^{13}	1.99×10^{12}	4.30×10^{10}	9.48×10^{11}
HCOO* → H_2COO* → H_2CO*					
R60	HCOO*H* ↔ H_2COO*	3.48×10^{12}	5.61×10^{13}	-	-
R61	H_2COO* ↔ H_2CO*O*	2.51×10^{12}	6.53×10^{12}	-	-
R62	H_2 + H_2CO*O* ↔ H_2CO*O*2H*	1.92×10^{08}	2.44×10^{14}	-	-
R63	H_2CO*O*2H* ↔ H_2CO*OH*H*	6.14×10^{11}	5.13×10^{12}	-	-
R64	H_2CO*OH*H* ↔ H_2CO*H_2O*	2.90×10^{13}	5.49×10^{11}	-	-
R65	H_2O* + H_2CO* ↔ H_2CO*H_2O*	6.42×10^{07}	1.00×10^{15}	-	-
Additional CO desorption					
R66	CO + 2H* ↔ CO*2H*	5.15×10^{07}	5.90×10^{16}	5.15×10^{07}	1.05×10^{15}

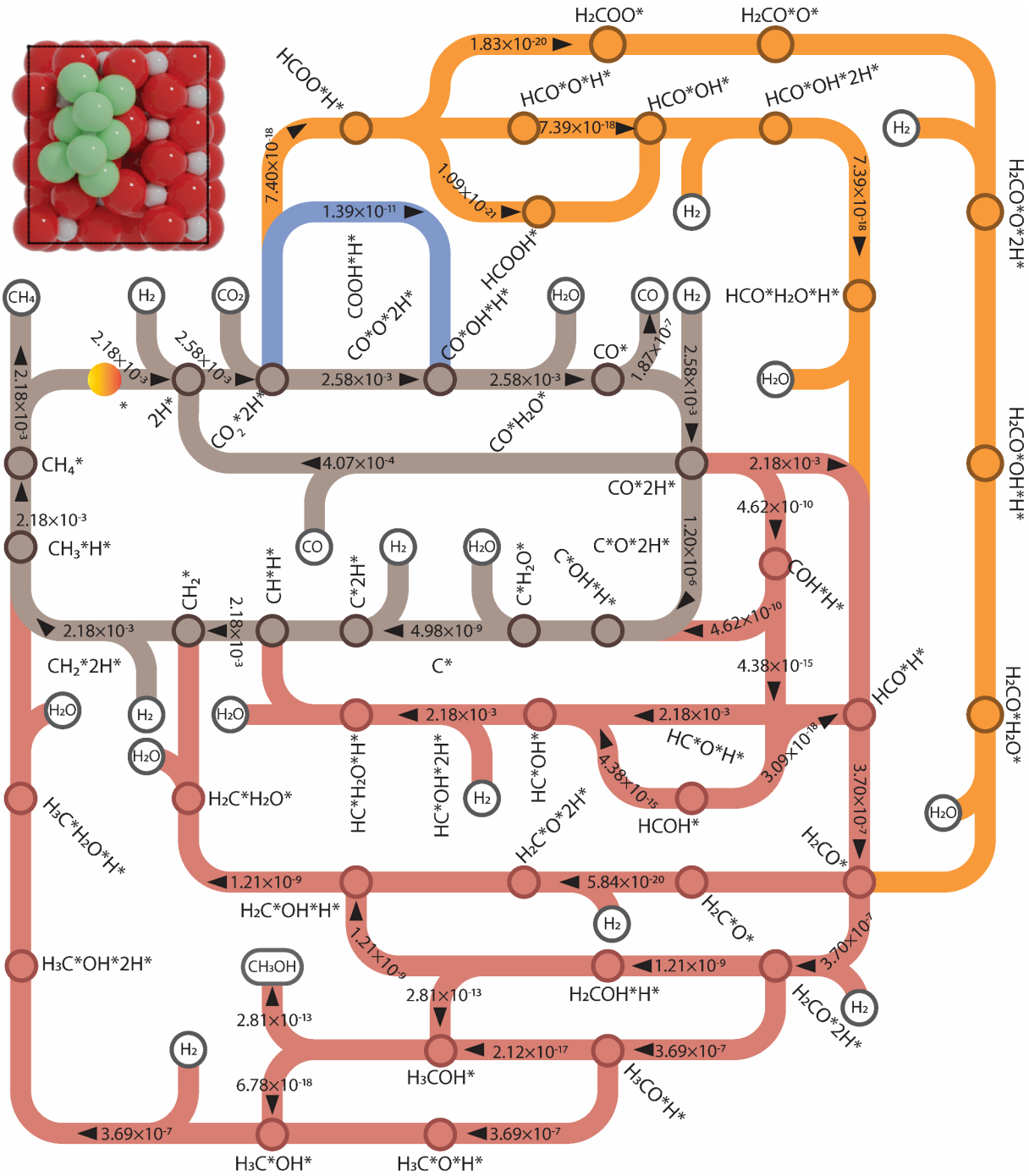

Figure S17. Fluxes of CO_2 hydrogenation on Ni_8/TiO_2-a surface at 600 K. The numbers given in the diagram are turnover rates (s^{-1}).

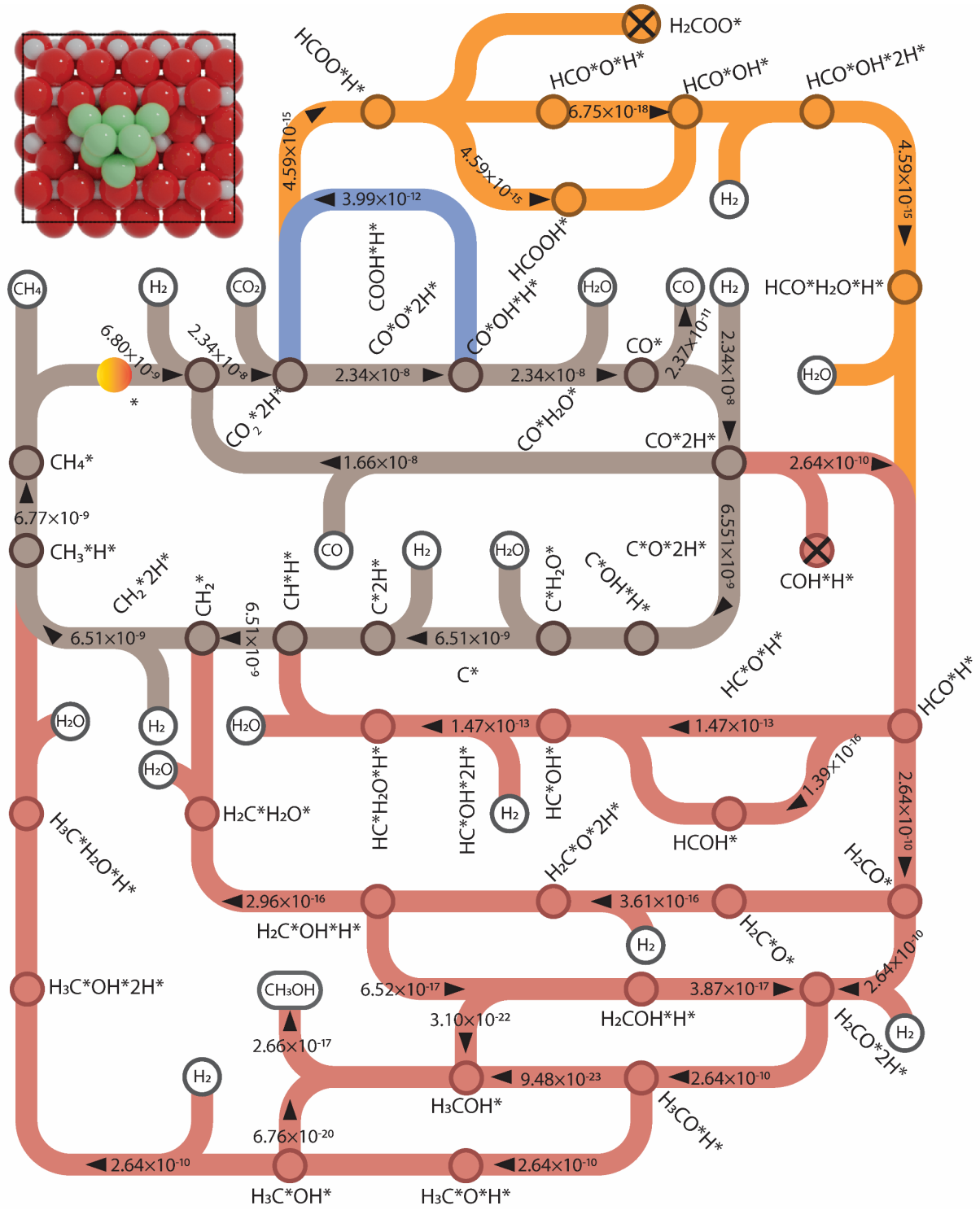

Figure S18. Fluxes of CO_2 hydrogenation on Ni_8/TiO_2-r surface at 600 K. The numbers given in the diagram are turnover rates (s^{-1}).

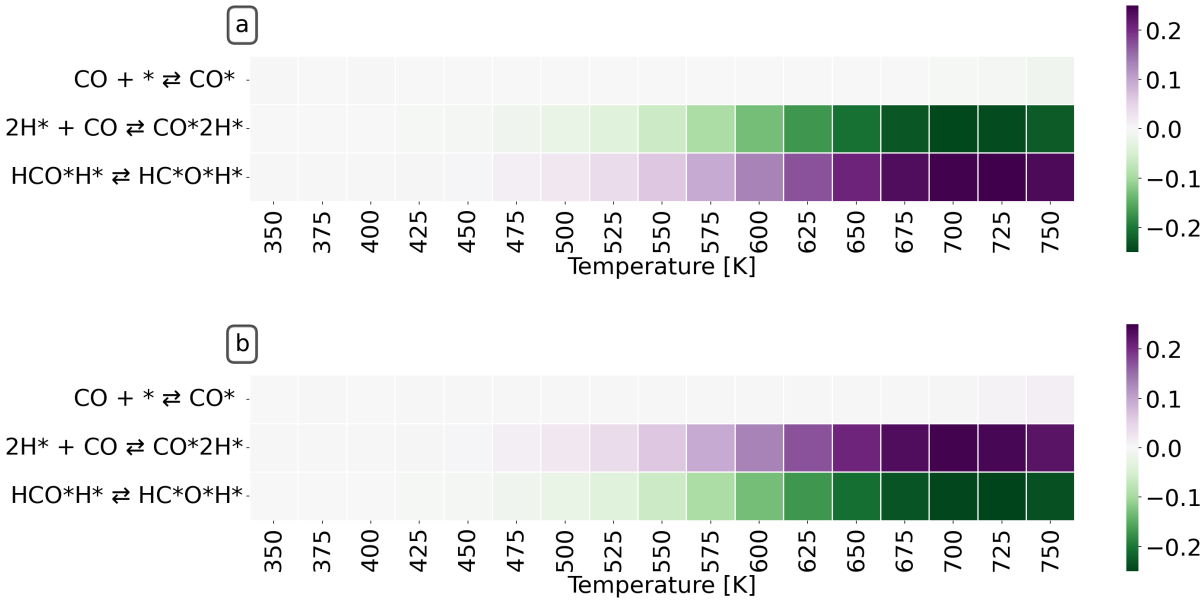

Figure S19. Degree of selectivity control (DSC) of (a) CH_4 and (b) CO formation as a function of temperature on Ni_8/TiO_2-a.

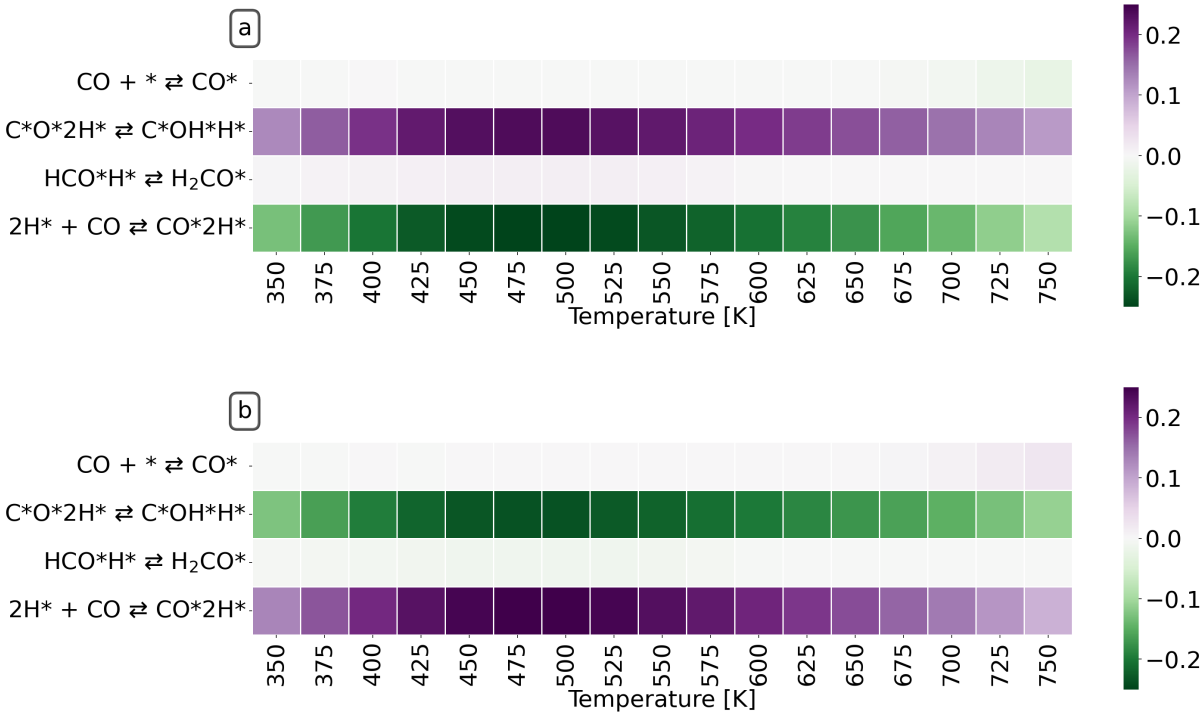

Figure S20. Degree of selectivity control (DSC) of (a) CH_4 and (b) CO formation as a function of temperature on Ni_8/TiO_2-r.

Table S3: Activation energies and reaction energies of direct CO dissociation on Ni_8/TiO_2 anatase and rutile as function of the number of co-adsorbed H* atoms. (energies in eV and ZPE correction is included)

	#H*	ΔE_{act}	ΔE_R
Ni_8/TiO_2 anatase	2	1.99	-0.24
	3	2.28	0.79
	4	2.50	1.00
Ni_8/TiO_2 rutile	2	1.41	0.33
	3	1.34	0.81
	4	1.71	1.13

Table S4: Activation energies and reaction energies of direct CO dissociation on Ni_8/TiO_2 anatase and rutile as function of the number of co-adsorbed H* atoms. (energies in eV and ZPE correction is included)

	#H*	Reaction	ΔE_{act}	ΔE_R	Overall activation energy
Ni_8/TiO_2 anatase	2	HCO formation	1.16	0.73	1.66
		HCO dissociation	0.93	-0.79	
	3	HCO formation	0.94	0.82	1.83
		HCO dissociation	1.01	-0.38	
	4	HCO formation	1.03	0.83	2.00
		HCO dissociation	1.17	-0.12	
Ni_8/TiO_2 anatase	2	HCO formation	1.52	1.18	2.84
		HCO dissociation	1.66	-0.60	
	3	HCO formation	1.02	0.51	2.49
		HCO dissociation	1.98	-0.14	
	4	HCO formation	1.34	0.60	2.67
		HCO dissociation	2.07	-0.01	

Additionally, the adsorption energy of H* was calculated to evaluate the possibility for a higher H* coverage. The results, summarized in Table R3, indicate that on both Ni_8/TiO_2 anatase and rutile surfaces, the adsorption of additional H* onto CO*2H* is less exothermic, particularly on Ni_8/TiO_2 rutile. Given the associated decrease in entropy during the adsorption process, the presence of 3H* and 4H* is deemed unlikely.

Table S5: The adsorption energy of H* on Ni_8/TiO_2 anatase and rutile. (energies in eV and ZPE correction is included)

	Reaction	$\Delta E_{R,\ forward}$	$\Delta E_{R,\ backward}$
Ni_8/TiO_2 anatase	$CO^* + H_2 \leftrightarrow CO^*2H^*$	0	1.46
	$CO^*2H^* + ½\ H_2 \leftrightarrow CO^*3H^*$	0	0.62
	$CO^*3H^* + ½\ H_2 \leftrightarrow CO^*3H^*$	0	0.47

Ni_8/TiO_2 rutile	$CO^* + H_2 \leftrightarrow CO^*2H^*$	0	1.78
	$CO^*2H^* + ½ H_2 \leftrightarrow CO^*3H^*$	0	0.22
	$CO^*3H^* + ½ H_2 \leftrightarrow CO^*3H^*$	0	0.53

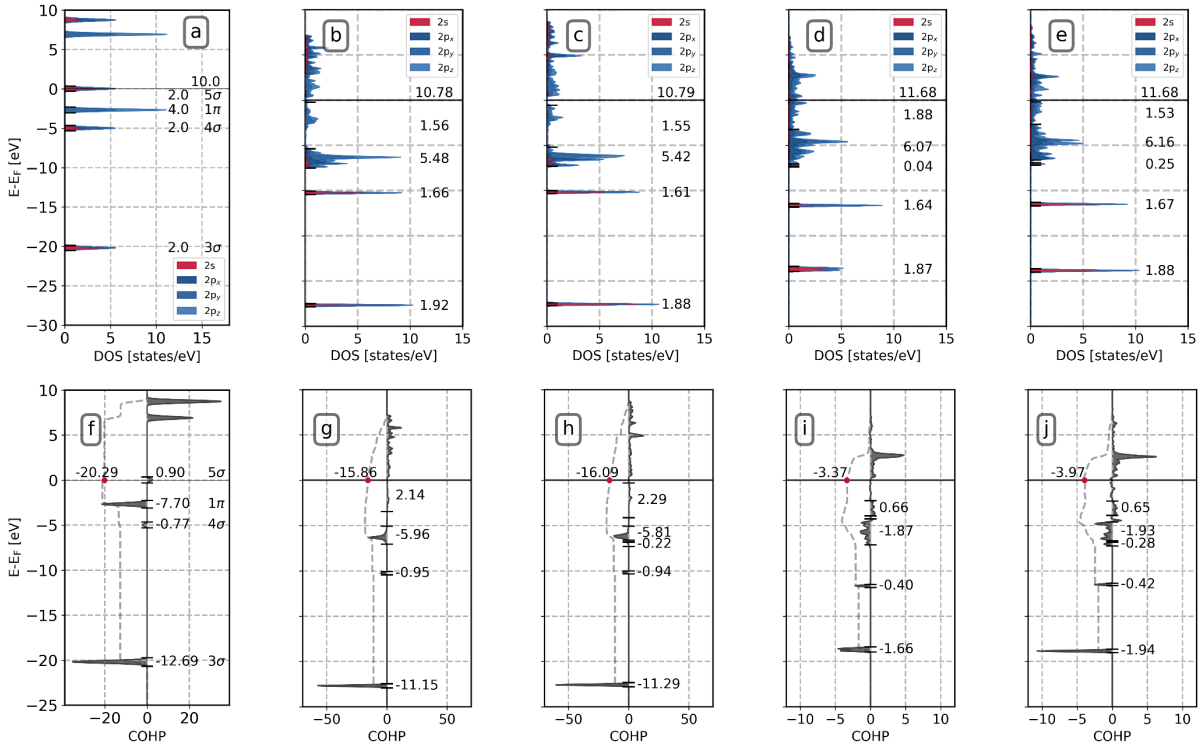

Figure S21. Analysis of DOS and COHP for gas-phase CO (a and f), adsorbed on Ni_8/TiO_2-a and Ni_8/TiO_2-r. The analysis includes both the initial state (IS) and transition state (TS) of CO direct dissociation on Ni_8/TiO_2-a and Ni_8/TiO_2-r. (a) to (e): DOS analysis; (f) to (j): COHP analysis. (b) and (g): IS on Ni_8/TiO_2-a; (c) and (i): IS on Ni_8/TiO_2-r; (d) and (h): TS on Ni_8/TiO_2-a; (e) and (j): TS on Ni_8/TiO_2-r. The numeric values above Fermi level indicate the integrated DOS (iDOS) and integrated COHP (iCOHP).

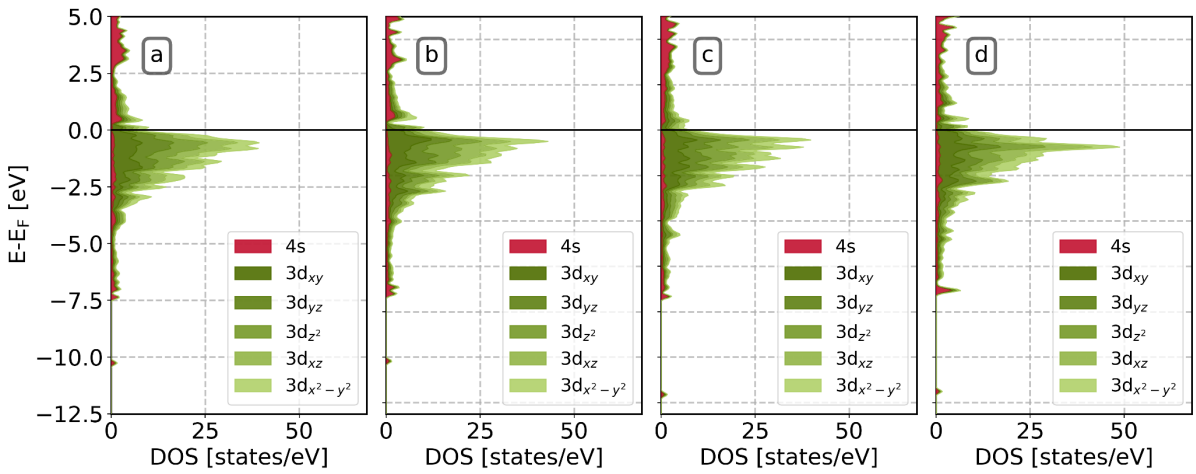

Figure S22. DOS analysis for Ni_8 clusters in the initial state (IS) and transition state (TS) of direct dissociation of CO* on both Ni_8/TiO_2-a and Ni_8/TiO_2-r. (a) IS on Ni_8/TiO_2-a; (b): IS on Ni_8/TiO_2-r; (c) TS on Ni_8/TiO_2-a; (d): TS on Ni_8/TiO_2-r. The numeric values above Fermi level indicate the integrated DOS (iDOS).

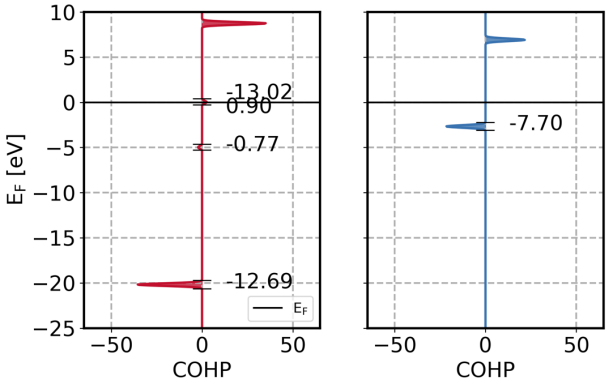

Figure S23. COHP of sigma (red) and pi (blue) orbitals for gas-phase CO.

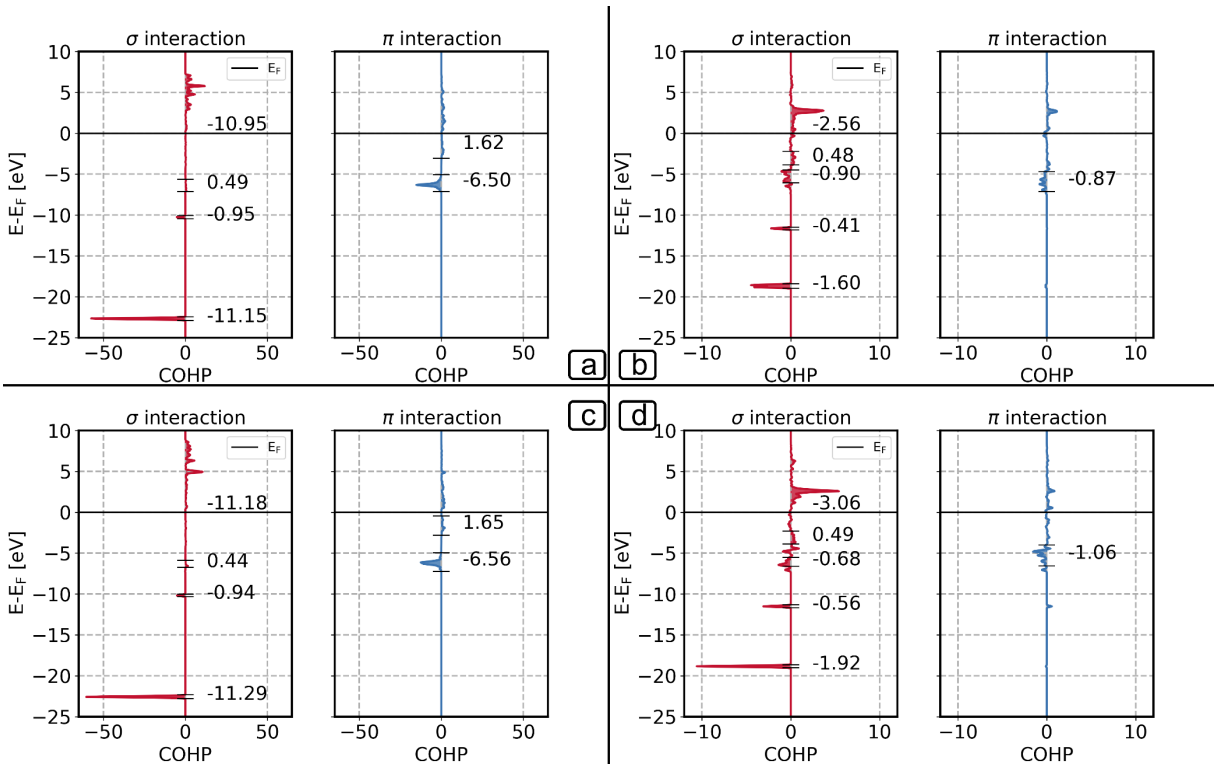

Figure S24. COHP of sigma (red) and pi (blue) orbitals for CO* dissociation on Ni_8/TiO_2-a and Ni_8/TiO_2-r. (a) IS on Ni_8/TiO_2-a; (b): IS on Ni_8/TiO_2-r; (c) TS on Ni_8/TiO_2-a; (d): TS on Ni_8/TiO_2-r.

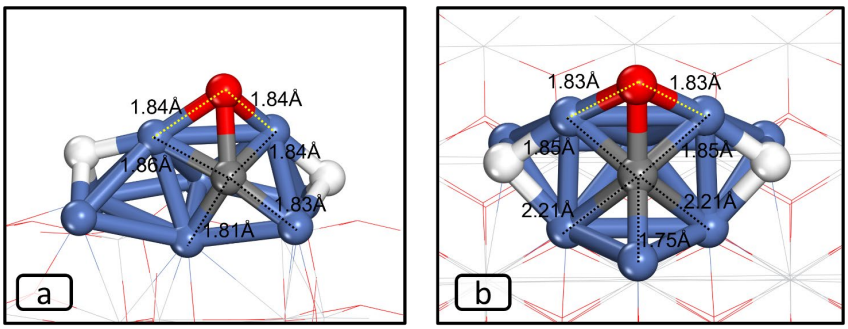

Figure S25. The location of C* and O* in the transition of CO* direct dissociation on (a) Ni_8/TiO_2-a and (b) Ni_8/TiO_2-r. The TiO_2 supports are depicted with lines to provide a clear visualization of the positions of C* and O* species. Color coding: blue: Ni; white: H; red: O; gray: C.

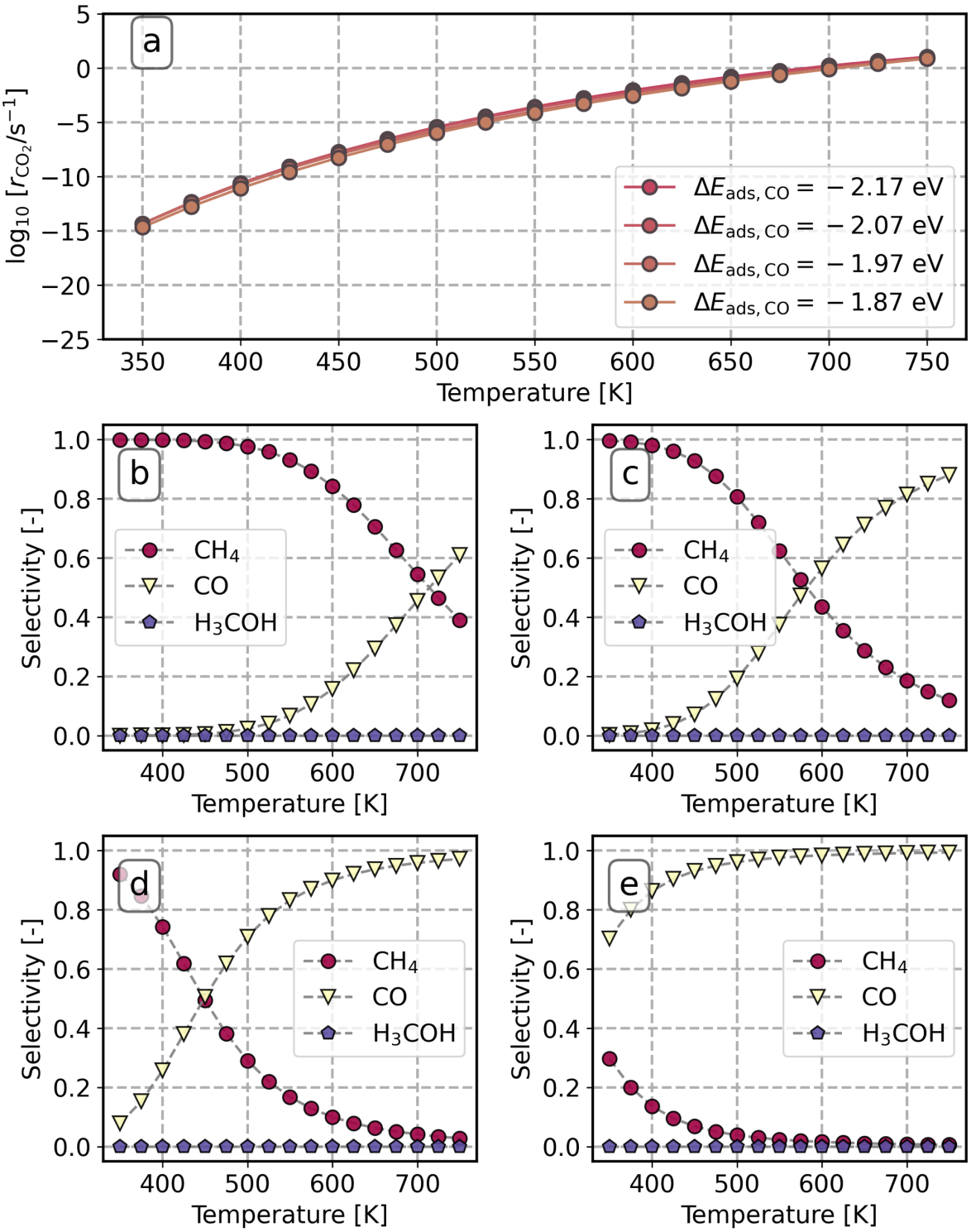

Figure S26. CO_2 reaction rate (a) and product distribution (b-e) as a function of temperature on Ni_8/TiO_2-a with varying CO adsorption energy. (b): $\Delta E_{ads,CO}$ = -2.17 eV; (c): $\Delta E_{ads,CO}$ = -2.07 eV; (d): $\Delta E_{ads,CO}$ = -1.97 eV; (e): $\Delta E_{ads,CO}$ = -1.87 eV.

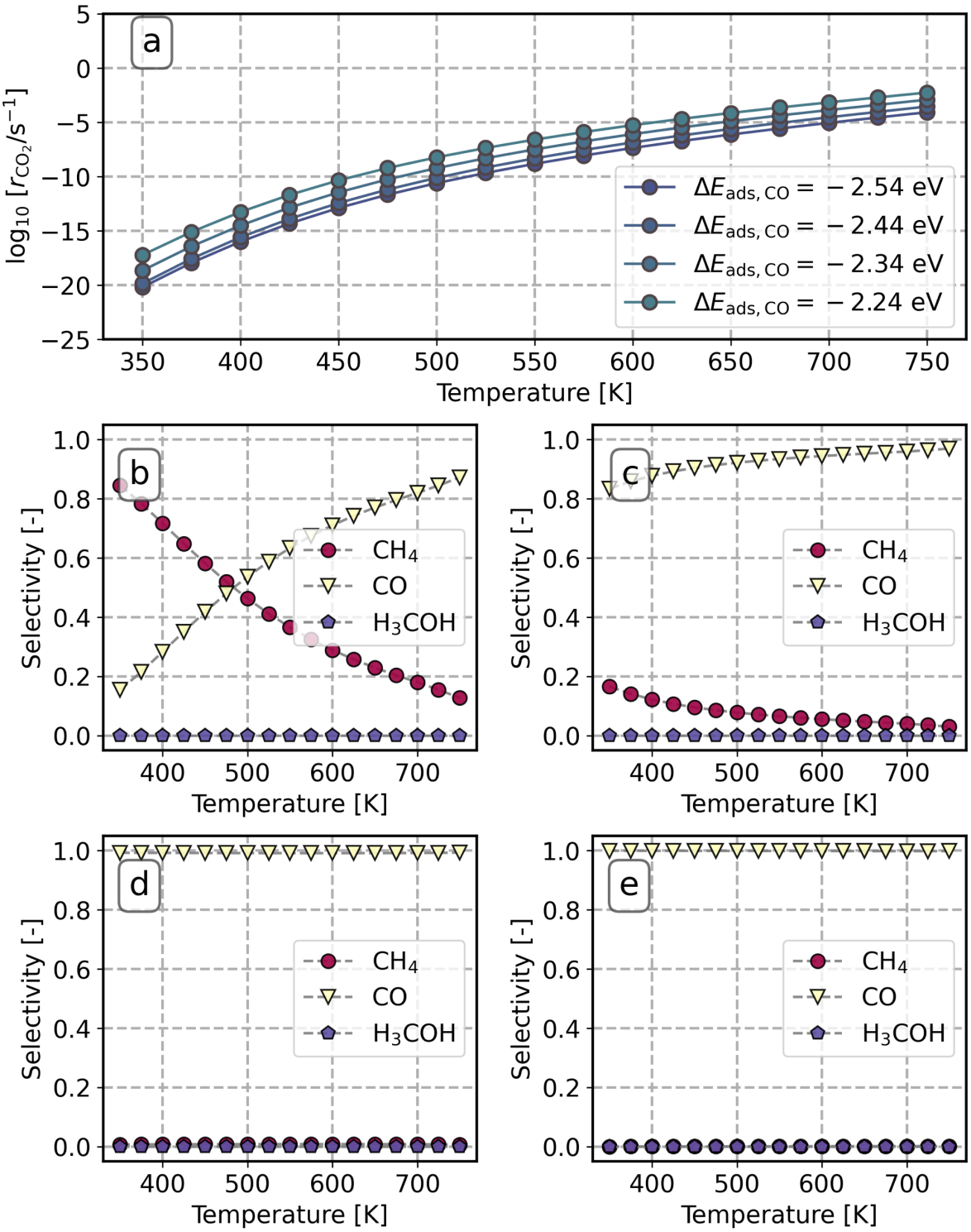

Figure S27. CO_2 reaction rate (a) and product distribution (b-e) as a function of temperature on Ni_8/TiO_2-r with varying CO adsorption energy. (b): $\Delta E_{ads,CO}$ = -2.54 eV; (c): $\Delta E_{ads,CO}$ = -2.44 eV; (d): $\Delta E_{ads,CO}$ = -2.34 eV; (e): $\Delta E_{ads,CO}$ = -2.24 eV.